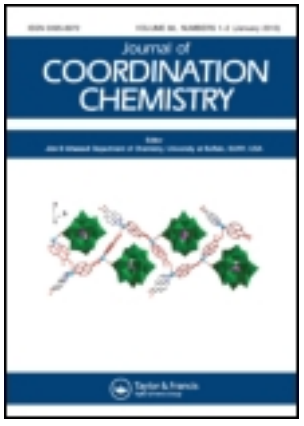

Journal of Coordination Chemistry
Publication details, including instructions for authors and subscription information:
http://www.tandfonline.com/loi/gcoo20

Synthesis and structural characterization of 2D Zn(II), Cd(II), and Co(II) coordination polymers containing 3-chloro-1,2-benzenedicarboxylate and positional isomers of triazole-bipyridine

Peng-Fei Yao [a], Chao-Jing Ye [a], Fu-Ping Huang [a], He-Dong Bian, Qing Yu [a] & Kun Hu [a]

[a] Department Chemistry and Chemical Engineering, Guangxi Normal University, Guilin, P.R. China

Accepted author version posted online: 18 Mar 2013.Published online: 29 Apr 2013.

To cite this article: Peng-Fei Yao, Chao-Jing Ye, Fu-Ping Huang, He-Dong Bian, Qing Yu & Kun Hu (2013) Synthesis and structural characterization of 2D Zn(II), Cd(II), and Co(II) coordination polymers containing 3-chloro-1,2-benzenedicarboxylate and positional isomers of triazole-bipyridine, Journal of Coordination Chemistry, 66:9, 1591-1601, DOI: 10.1080/00958972.2013.784746

To link to this article: http://dx.doi.org/10.1080/00958972.2013.784746

Journal of Coordination Chemistry, 2013
Vol. 66, No. 9, 1591–1601, http://dx.doi.org/10.1080/00958972.2013.784746

Synthesis and structural characterization of 2D Zn(II), Cd(II), and Co(II) coordination polymers containing 3-chloro-1,2-benzenedicarboxylate and positional isomers of triazole-bipyridine

PENG-FEI YAO, CHAO-JING YE, FU-PING HUANG*, HE-DONG BIAN, QING YU* and KUN HU

Department Chemistry and Chemical Engineering, Guangxi Normal University, Guilin, P.R. China

(*Received 30 September 2012; in final form 8 February 2013*)

Three compounds, $[Zn_2L_2(4,4'\text{-bpt})_2]_n$ (**1**), $[Cd_2L_2(3,4'\text{-bpt})(H_2O)_2]_n$ (**2**) and $\{[CoL(3,3'\text{-bpt})(H_2O)]\cdot H_2O\}_n$ (**3**) (L = 3-Cl-1,2-benzenedicarboxylate dianion, 4,4′-bpt = 1H-3,5-bs(4-pyridyl)-1,2,4-itriazole, 3,4′-bpt = 1H-3-(3-pyridyl)-5-(4-pyridyl)-1,2,4-triazole and 3,3′-bpt = 1H-3,5-bis(3-pyridyl)-1,2,4-triazole), based on three positionally isomeric triazole-bipyridine ligands, were synthesized. Structural analyses of **1–3** reveal diverse 2-D network structures, which are based on different $[ML]_n$ (M = Zn, Cd, Co) chains. In the $[ZnL]_n$ chains of **1**, the carboxylic groups of L connect the adjacent Zn(II) centers with a monodentate bridging coordination mode (μ_2-η^1/η^1). In **2**, $[CdL]_n$ is a double chain connected by the carboxylic groups of L with μ_3-$\eta^1/\eta^2/\eta^2$ and μ_3-$\eta^1/\eta^1/\eta^2$ bridges. The $[CoL]_n$ chains of **3** are formed by the carboxylic groups of L with the μ_2-η^1/η^2 coordination mode. The powder X-ray diffraction and the thermal stability of **1–3**, the luminescent properties of **1** and **2**, and the magnetic behavior of **3** have been briefly investigated.

Keywords: Positional isomeric ligands; Crystal structures; Luminescence properties; Magnetic properties

1. Introduction

The design and preparation of polynuclear compounds have received attention during recent years, not only because of their various structural topologies but also because of their potential applications in luminescence, catalysis, gas adsorption, and especially, magnetochemistry [1, 2]. The structures of coordination polymers are determined by several factors, including the coordination geometry of the central metal ions, solvents [3], ligand structure, metal/ligand ratio [4], counterions [5], pH and temperature [6]. Rational design of ligands is usually a useful and important way to study the controlled synthesis of a molecular architecture. With this understanding, one crucial aim of this work was to explore the essential factors of positional isomeric ligands for regulating the structural assembly, which may provide further insights in designing new hybrid crystalline materials

*Corresponding authors. Email: huangfp2010@163.com (F.-P. Huang); gxnuchem312@yahoo.com.cn (Q. Yu)

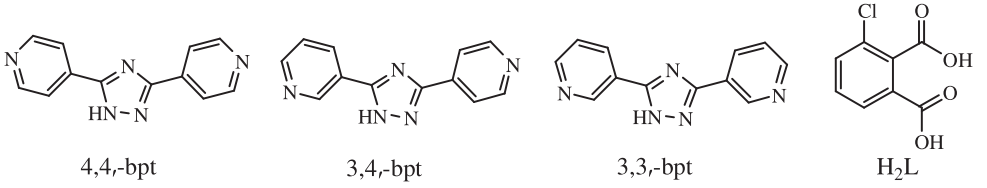

Chart 1. The ligands used in this work: positionally isomeric bridging ligands 4,4′-bpt, 3,4′-bpt, and 3,3′-bpt and the carboxylic diacid ligand H_2L.

[7]. Because an accurate prediction of the final structure is currently impossible, the exploration of the positional isomeric factors for the ultimate structures is not trivial [8].

Herein, we report three different 2-D coordination polymers produced by H_2L and three positionally isomeric ligands (4,4′-bpt, 3,4′-bpt, and 3,3′-bpt) (chart 1). Structural analyses reveal that the benzenedicarboxylate dianions display versatile coordination modes to arrange the Zn(II), Cd(II), and Co(II) ions into different forms of infinite chains, which are further extended via the isomeric bpt connectors in different directions, to give a variety of coordination polymers. This work indicates that the versatile coordination modes of L (Scheme 1), the isomeric effects of the bpt ligands, and the different coordination geometries of the central metal ions are significant in the construction of these network structures. Moreover, the powder X-ray diffraction (PXRD) of **1**–**3**, the thermal stability and the luminescent properties of **1** and **2**, and the magnetic behavior of **3** have been briefly investigated [9].

2. Experimental

With the exception of the ligands 4,4′-bpt, 3,4′-bpt, and 3,3′-bpt, which were prepared according to the literature procedure [10], all reagents and solvents for synthesis and analysis were commercially available and used as received. Elemental analyses were performed on a CE-440 (Leemanlabs) analyzer. Fourier transform (FT) IR spectra (KBr pellets) were acquired on an AVATAR-370 (Nicolet) spectrometer. PXRD patterns were measured on a Rigaku D/max-IIIA diffractometer (Mo-Kα $\lambda = 0.71073$ Å). The single-crystalline powder samples were prepared by crushing the crystals and scanned from 3 to 60° with a step of 0.1 s^{-1}. Calculated patterns of **1**–**3** were generated with PowderCell.

2.1. *Preparation of $[Zn_2L_2(4,4'\text{-bpt})_2]_n$ (1)*

A mixture containing $ZnCl_2$ (68 mg, 0.5 mmol), 4,4′-bpt (112 mg, 0.5 mmol), H_2L (100 mg, 0.5 mmol), NaOH (40 mg, 1 mmol), water (10 mL) and ethanol (5 mL) was sealed in a

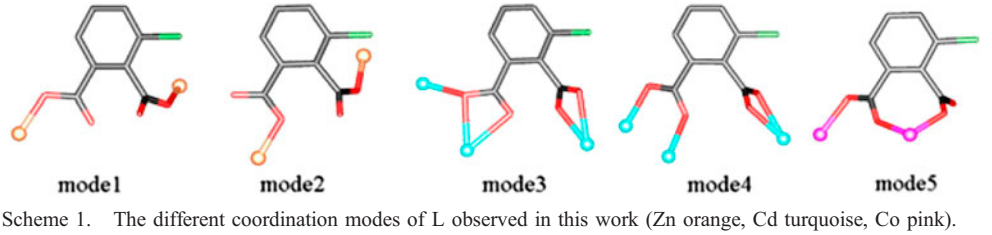

Scheme 1. The different coordination modes of L observed in this work (Zn orange, Cd turquoise, Co pink).

Teflon-lined stainless steel vessel (23 mL), heated at 140 °C for 3 days and then cooled to room temperature at a rate of 5 °C/h. Colorless block crystals of **1** (yield 44%, based on Zn) were obtained and picked out, washed with distilled water and dried in air. Elemental analysis for $C_{40}H_{24}Cl_2N_{10}O_8Zn_2$ (%) Calcd: C, 49.28; H, 2.46; N, 14.37; Cl, 7.29. Found: C, 49.69; H, 2.72; N, 14.48; Cl, 7.23. IR (KBr, cm^{-1}): 3054s, 1624w, 1497s, 1450m, 1371w, 1031w, 844m, 735m, 554s.

2.2. *Preparation of $[Cd_2L_2(3,4'\text{-bpt})(H_2O)_2]_n$ (2)*

The same synthetic procedure as that for **1** was used except that 4,4′-bpt and $ZnCl_2$ was replaced by 3,4′-bpt and $CdCl_2$, respectively, giving colorless block X-ray quality crystals of **2** in a 45% yield (based on Cd). Anal. Calcd for $C_{28}H_{19}Cd_2Cl_2N_5O_{10}$: C, 38.14; H, 2.16; N, 7.95. Found: C, 38.04; H, 2.37; N, 7.98. IR (cm^{-1}): 3074m, 1575w, 1550w, 1462m, 1448m, 1388w, 842s, 787s, 731m, 699s.

2.3. *Preparation of $\{[CoL(3,3'\text{-bpt})(H_2O)]\cdot H_2O\}_n$ (3)*

The same synthetic procedure as that for **1** was used except that 4,4′-bpt and $ZnCl_2$ was replaced by 3,3′-bpt and $CoCl_2$, respectively, giving red block X-ray quality crystals of **3** in a 35% yield (based on Co). Anal. Calcd for $C_{20}H_{16}ClCoN_5O_6$: C, 46.21; H, 3.09; N, 13.54. Found: C, 46.33; H, 3.26; N, 13.68. IR (cm^{-1}): 3406m, 3055m, 1671s, 1599w, 1574s, 1544w, 1456m, 1400w, 1369m, 1144s, 1053s, 705s.

2.4. *X-ray structure determination*

X-ray single-crystal diffraction data for **1–3** were collected with a Bruker SMART CCD instrument by using graphite monochromated Mo-Kα radiation (λ = 0.71073 Å). The data were collected at 293(2) K, and there was no evidence of crystal decay during data collection. A semi-empirical absorption correction was applied using SADABS, and the program SAINT was used for integration of the diffraction profiles. The structures were solved by direct methods with SHELXS-97 and refined by full-matrix least-squares methods on all F^2 data with SHELXL-97 [11]. The non-hydrogen atoms were refined anisotropically. Hydrogens bound to carbon and nitrogen were placed geometrically and allowed to ride during the subsequent refinements with isotropic displacement parameters. The starting positions for hydrogen atoms of water molecules were located in the difference maps and then fixed in the given positions. The final cycle of full-matrix least-squares refinement was based on observed reflections and variable parameters. Crystallographic data and structural refinement details are summarized in table 1. Selected bond lengths and angles are given in table 2.

3. Description of the crystal structures

3.1. *$[Zn_2L_2(4,4'\text{-bpt})_2]_n$ (1)*

Single-crystal X-ray structural analysis shows that the structure of **1** is a 2-D layer complex containing two crystallographically independent Zn atoms (figure 1). Both Zn_1

Table 1. Crystal data and structure refinement parameters for **1–3**.

	1	**2**	**3**
Empirical formula	$C_{40}H_{24}Cl_2N_{10}O_8Zn_2$	$C_{28}H_{19}Cd_2Cl_2N_5O_{10}$	$C_{20}H_{16}ClCoN_5O_6$
Formula weight (M)	974.37	881.20	516.76
Crystal system	Monoclinic	Triclinic	Triclinic
Space group	$P21/c$	P-1	P-1
a (Å)	12.865(3)	7.5040(15)	8.7780(18)
b (Å)	14.623(3)	10.379(2)	10.436(2)
c (Å)	20.172(4)	20.328(4)	12.819(3)
α (°)	90.00	99.25(3)	109.54(3)
β (°)	97.44(3)	99.58(3)	90.49(3)
γ (°)	90.00	103.75(3)	114.26(3)
V (Å^3)	3762.9(13)	1482.9(5)	994.3(5)
Z	4	2	2
D_c (Mg m^{-3})	1.720	1.974	1.726
F(000)	2415	864	858
θ range for data collection (°)	25.25	27.45	25.25
Reflections collected/unique	21,136 / 6756 [R(int) = 0.086]	12,602 / 6706 [R(int) = 0.025]	5898 / 3566 [R(int) = 0.051]
Goodness-of-fit on F^2	1.072	0.992	1.008
Final R indices [$I > 2\sigma(I)$]	$R_1 = 0.0711$ $\omega R_2 = 0.1330$	$R_1 = 0.0319$ $\omega R_2 = 0.0925$	$R_1 = 0.0699$ $\omega R_2 = 0.1328$
R indices (all data)	$R_1 = 0.1079$ $\omega R_2 = 0.1474$	$R_1 = 0.0374$ $\omega R_2 = 0.0955$	$R_1 = 0.1062$ $\omega R_2 = 0.1499$

and Zn_2 are coordinated by two N atoms from two 4,4′-bpt ligands and two carboxylate O atoms from two different L ligands to yield a distorted tetrahedral geometry. The Zn–O/N distances fall in the range 1.908(4)–2.076(5) Å, consistent with corresponding reported values [12]. The adjacent Zn(II) centers are linked by the carboxylic groups of L with monodentate coordination mode (scheme 1, mode 1, mode 2) to form infinite $[ZnL]_n$ chains ($Zn \cdots Zn = 6.884(1)$ Å) running along the crystallographic a axis. The Zn(II) centers are also bridged to neighboring $[ZnL]_n$ chains by a bent 4,4′-bpt ligand to generate zigzag chains with a $Zn \cdots Zn$ distance of 14.000(3) Å. The two types of chains intersect at the Zn atoms and give rise to a wave-like layer structure.

3.2. *$[Cd_2L_2(3,4'\text{-bpt})(H_2O)_2]_n$ (2)*

The fundamental building unit of $[Cd_2L_2(3,4'\text{-bpt})(H_2O)_2]_n$ (figure 2) contains two independent Cd(II) centers. The Cd1 atom is seven-coordinate with a distorted pentagonal bipyramidal coordination sphere, defined by one carboxylate O atom and one nitrogen from 3,4′-bpt occupying the axial positions, while four carboxylate O atoms from three L and one O atom from a coordinated water molecule occupy the equatorial positions. The Cd2 atom adopts a distorted octahedral geometry and is coordinated by one O atom from a coordinated water molecule and one N atom from 3,4′-bpt, occupying the axial positions, and four carboxylate O atoms from three L ligands, occupying the equatorial positions. The monodentate Cd–O(water) and Cd–N bond distances range from 2.317(3) to 2.366(3) Å. In **2**, L displays two coordination modes, μ_3-$\eta^1/\eta^2/\eta^2$ (Scheme 1, mode 3) and μ_3-$\eta^1/\eta^1/\eta^2$ (scheme 1, mode 4). In the former mode, consisting of atoms O1, O2, O3, and O4, O2 asymmetrically bridges Cd1 and Cd2 (Cd1–O1, 2.481(3) Å; Cd2–O2B, 2.215 (3) Å), while the remaining Cd–O distances are between 2.340(3) and 2.481(3) Å. In the latter mode, formed with atoms O5, O6, O7, and O8, both chelating carboxylates show asymmetric binding to their respective Cd atoms (Cd1–O5, 2.271(3) and Cd1–O6, 2.569

Table 2. Selected bond distances (Å) and angles (°) for **1–3**.

1 (Symmetry codes: A: $x+1$, $-y+1/2$, $z+1/2$; B: x, $-y+1/2$, $z-1/2$; C: $x-1$, y, z)			
Zn1–O1	1.908(4)	Zn2–O7	1.931(4)
Zn1–O5	1.951(4)	Zn2–O4C	1.933(4)
Zn1–N10A	2.021(5)	Zn2–N6	2.040(4)
Zn1–N5B	2.053(4)	Zn2–N1	2.076(5)
O1–Zn1 O5	124.6(2)	O7–Zn2–O4C	114.2(2)
O1–Zn1–N10A	121.0(2)	O7–Zn2–N6	122.3(2)
O5–Zn1–N10A	100.0(2)	O4C– n2–N6	112.9(2)
O1– n1–N5B	96.8(2)	O7 Zn2–N1	103.2(2)
O5–Zn1–N5B	106.4(2)	O4C–Zn2–N1	95.5(2)
N10A–Zn1–N5B	106.2(2)	N6–Zn2–N1	103.5(2)
2 (Symmetry codes: A: $-x$, $-y+2$, $-z+1$; B: $x+1$, y, z; C: $-x+1$, $-y+2$, $-z+1$; D: $-x+1$, $-y+2$, $-z$)			
Cd1–O5	2.271(3)	Cd2–O2B	2.215(3)
Cd1–N1	2.317(3)	Cd2–O8C	2.218(3)
Cd1–O7A	2.359(3)	Cd2–O10	2.328(3)
Cd1–O9	2.366(3)	Cd2–O3	2.340(3)
Cd1–O2	2.470(3)	Cd2–N5D	2.347(3)
Cd1–O1	2.481(3)	Cd2–O4	2.467(3)
Cd1–O6	2.569(3)		
O5–Cd1–N1	176.2(1)	O9–Cd1–O6	73.2(1)
O5–Cd1–O7A	92.5(1)	O2–Cd1–O6	117.7(1)
N1–Cd1–O7A	89.7(1)	O1–Cd1–O6	77.6(1)
O5–Cd1–O9	94.0(1)	O2B–Cd2–O8C	111.2(1)
N1–Cd1–O9	83.3(1)	O2B–Cd2–O10	81.7(1)
O7A–Cd1–O9	81.9(1)	O8C–Cd2–O10	90.4(1)
O5–Cd1–O2	88.5(1)	O8C–Cd2–O3	100.0(1)
N1–Cd1–O2	94.7(1)	O10–Cd2–O3	104.1(1)
O7A–Cd1–O2	85.8(1)	O2B–Cd2–N5D	93.1(1)
O9–Cd1–O2	167.5(1)	O8C–Cd2–N5D	89.2(1)
O5–Cd1–O1	90.4(1)	O10–Cd2–N5D	174.3(1)
N1–Cd1–O1	90.0(1)	O3–Cd2–N5D	81.6(1)
O7A–Cd1–O1	137.6(1)	O2B–Cd2–O4	99.2(1)
O2–Cd1–O1	52.1(1)	O8C–Cd2–O4	143.7(1)
O5–Cd1–O6	54.2(1)	O10–Cd2–O4	74.5(1)
N1–Cd1–O6	122.3(1)	O3–Cd2–O4	54.4(1)
O7A–Cd1–O6	135.4(1)	N5D–Cd2–O4	108.9(1)
3 (Symmetry codes: A: $-x+2$, $-y+1$, $-z$; B: $-x+2$, $-y$, $-z$; C: x, $y-1$, $z-1$; D: $-x+2$, $-y+1$, $-z+1$)			
Co1–O1	2.023(4)	Co2–O5	2.076(4)
Co1–O3	2.074(4)	Co2–O4	2.099(3)
Co1–N1	2.189(4)	Co2–N5C	2.114(4)
O1–Co1–O3	90.4(2)	O5B–Co2–O4	90.9(2)
O1A–Co1–O3	89.6(2)	O5–Co2–O4	89.1(2)
O1–Co1–N1	90.8(2)	O5B–Co2–N5C	89.6(2)
O3–Co1–N1	89.8(2)	O4–Co2–N5C	90.3(2)

(3) Å; Cd2-O7A, 2.359(3) and Cd2–O8C, 2.218(3) Å). While the Cd1–O6 bond distance can be described as a semi-chelating coordination, all bond distances are consistent with reported values [13]. The carboxylates of L connect the neighboring Cd1 and Cd2 atoms to form an infinite double chain running along the *a* axis. The neighboring double chains are further connected by the 3,4′-bpt ligands running along the *c* axis to form a 2-D network structure.

3.3. *{[CoL(3,3′-bpt)(H$_2$O)]·H$_2$O}$_n$ (3)*

Compound **3** has a polymeric layer structure containing two crystallographically independent Co atoms (figure 3) [14]. Both Co(II) ions sit on inversion centers and have

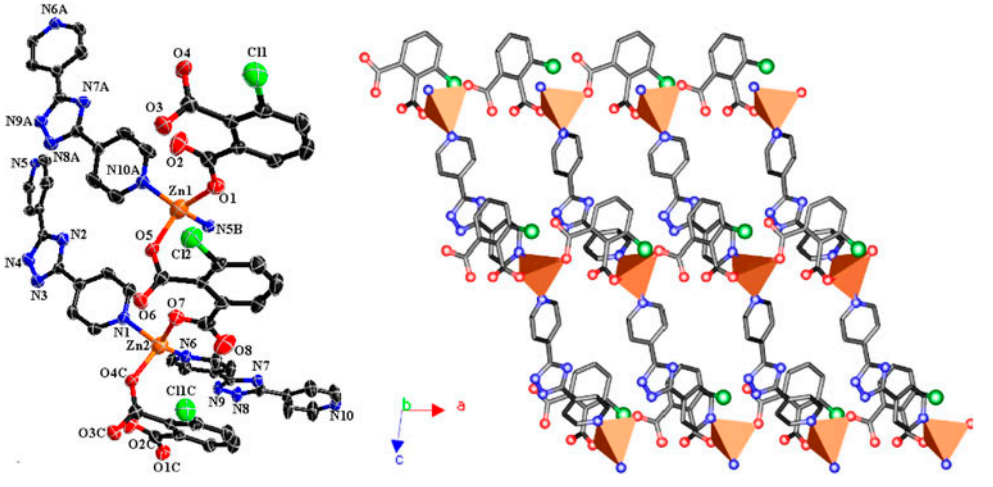

Figure 1. Structure of **1** (50% probability thermal ellipsoids) showing the local coordination environments of the Zn(II) centers (left) and the 2-D network (right). Symmetry codes: A: $x+1$, $-y+1/2$, $z+1/2$; B: x, $-y+1/2$, $z-1/2$; C: $x-1$, y, z.

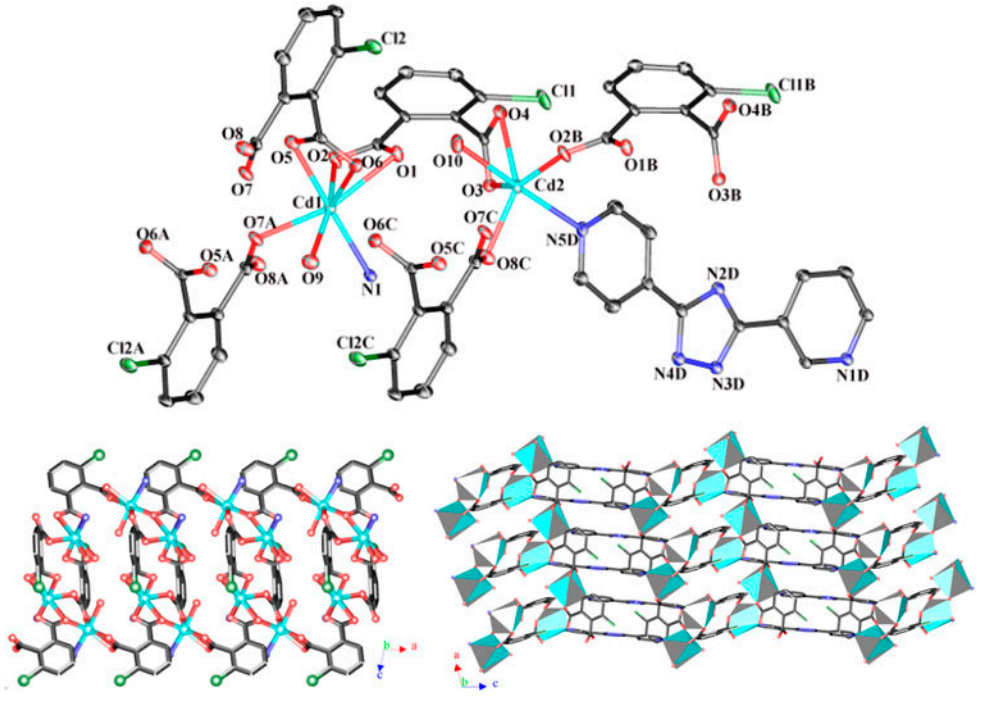

Figure 2. Structure of **2** (30% probability ellipsoids) showing the local coordination environment of the Cd atoms (top), the infinite $[CdL]_n$ chain (bottom left), and the 2-D network (bottom right). Symmetry codes: A: $-x$, $-y+2$, $-z+1$; B: $x+1$, y, z; C: $-x+1$, $-y+2$, $-z+1$; D: $-x+1$, $-y+2$, $-z$.

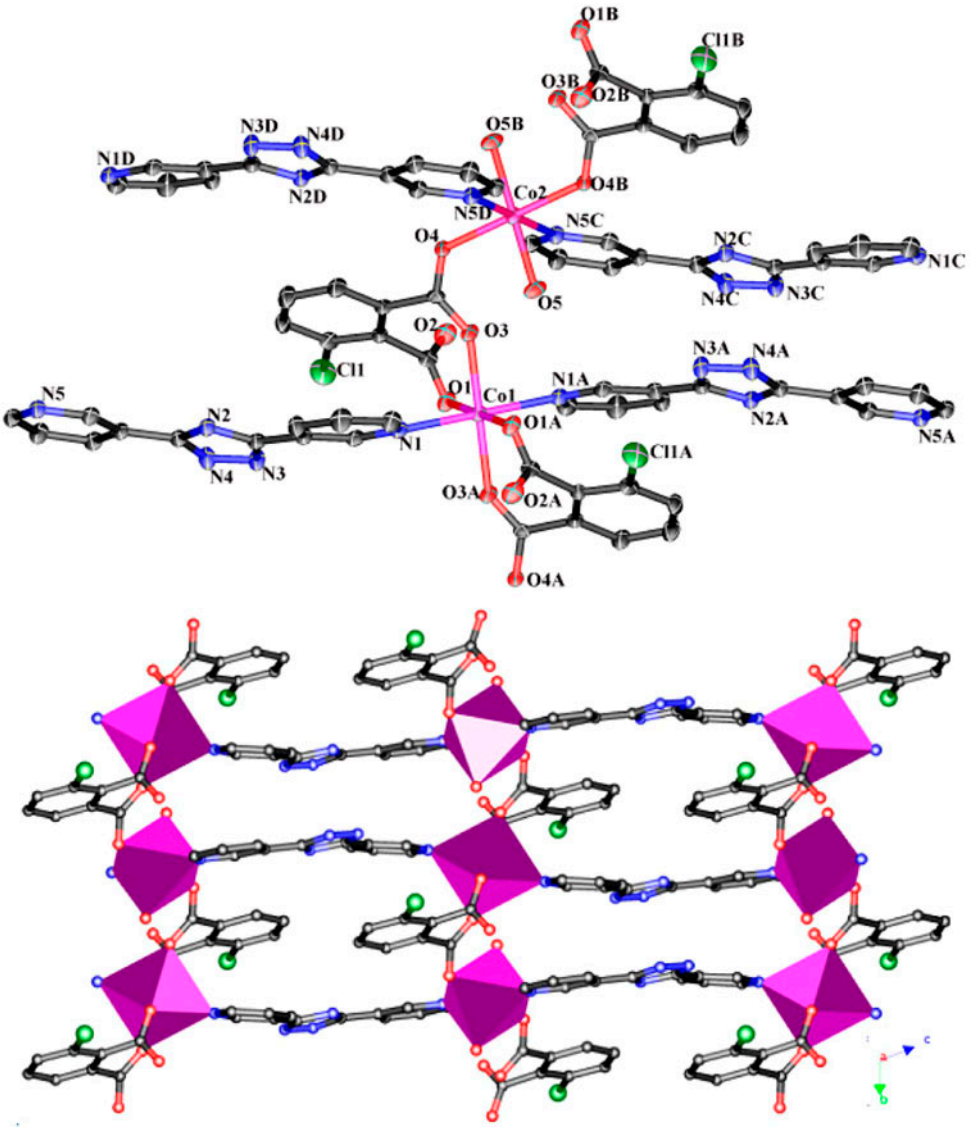

Figure 3. Structure of **3** (30% probability ellipsoids) showing the local coordination environments of the Co(II) atoms (top) and the 2-D network (bottom). Symmetry codes: A: $-x+2$, $-y+1$, $-z$; B: $-x+2$, $-y$, $-z$; C: x, $y-1$, $z-1$; D: $-x+2$, $-y+1$, $-z+1$.

octahedral configurations. Co1 is coordinated by two pyridine N atoms from two 3,3′-bpt ligands, occupying axial positions, and four carboxylate O atoms from two L, occupying the equatorial positions. Co2 is coordinated by two pyridine N atoms from two 3,3′-bpt ligands, occupying axial positions, and two carboxylate O atoms from two L and two O atoms from water molecules, which occupy the equatorial positions. The Co–O/N distances fall in the range 2.023(4)–2.189(4) Å, consistent with reported values [15]. In **3**, L adopts a μ_2-η^1/η^2 coordination mode (scheme 1, mode 5), linking adjacent Co(II) ions to form an infinite chain with Co···Co separation of 5.218(2) Å. The linear $[CoL]_n$ chain is further

perpendicularly pillared by the *trans*-coordinated 3,3′-bpt ligand to afford a 2-D framework with interchain Co···Co separation of 12.116(2) Å.

3.4. *Structural diversity of 1–3*

In **1–3**, the metal centers were linked by L to form three different infinite chains, which were further extended by the isomeric bpt connectors in different directions. The structural diversification in **1–3** may originate from three different sources. (i) The aromatic linker L with two adjacent carboxylate groups can adopt various coordination modes. In **1**, the carboxylate groups of L have a monodentate coordination mode (Scheme 1, mode 1, mode 2). In **2**, L displays μ_3-$\eta^1/\eta^2/\eta^2$ and μ_3-$\eta^1/\eta^1/\eta^2$ coordination modes (Scheme 1, mode 3, mode 4). In **3**, L has a μ_2-η^1/η^2 coordination mode (Scheme 1, mode 5). (ii) The coordinated geometries of different metal centers may play significant roles in the formation of different structures [16]. In **1**, the Zn(II) center adopts a distorted tetrahedral geometry. In **2**, Cd1 has a seven-coordinate, distorted pentagonal bipyramidal coordination sphere, while Cd2 has a distorted octahedral geometry. In **3**, the Co(II) centers adopt octahedral configurations. (iii) The differently oriented pyridyl N atoms in these triazole-containing isomers, which have bent backbones, may benefit the structural diversification [17]. While not observed in **1–3**, the N atoms of triazole ring can provide potential coordination or hydrogen-bonding sites that will influence the final coordination architectures. Comparing the structural features of **3** with the previously reported polymers $\{[CoL(3,4'\text{-bpt})]\}_n$ and $\{[CoL(4,4'\text{-bpt})(H_2O)]\}_n$ [7], the Co···Co distances are 12.116(2), 13.943(5) and 14.093 (2) Å, respectively, although the bpt isomers only behave as connectors between infinite chains, as shown in **3**. With respect to crystal engineering, our previous studies [7,9,18] showed that the dicarboxylate ligands generally link the metal centers to form various infinite chains, and the further extension of the arrays in different directions by the isomeric bpt connectors gives rise to their final structural diversities, which, however, cannot be accurately forecasted [18g].

4. Physical properties of 1–3

4.1. *XRPD results*

In order to confirm the phase purity of the samples, PXRD experiments have been carried out for **1–3**. The PXRD experimental and computer-simulated patterns for **1–3** are shown in figure S1. Although the experimental patterns have a few unindexed diffraction lines and some lines are slightly broadened in comparison with those simulated from the single crystal models, **1–3** can be considered to be phase pure [15].

4.2. *The solid-state emission spectra of 1 and 2*

Compounds constructed by Zn(II) or Cd(II) centers and conjugated organic linkers are promising candidates for photoactive materials with potential applications within photochemistry and sensor technology [20]. Therefore, solid-state fluorescence spectra of **1** and **2** were recorded at room temperature (see figure S2). The bpt isomers ligands show very similar emission bands at $\lambda_{max} = 364$ nm ($\lambda_{ex} = 327$ nm) which agree well with our previously reported studies [7,9,18a]. Upon complexation of these ligands with Zn(II) and Cd(II) atoms, strong luminescence was observed in the solid state at room temperature. For **1** and **2**, the

maximum emission bands are at 414 nm (λ_{ex} = 358 nm) and 392 nm (λ_{ex} = 314 nm), respectively, and these likely arise from intraligand $\pi \rightarrow \pi^*$ transitions [21]. The red-shift for such fluorescence peaks of the maximum emission bands, compared with that of the free bpt isomers, is the result of the incorporation of metal-ligand coordination interactions [22]. Moreover, the luminescence enhancement may be due to the chelating and/or bridging effects of the ligands to the Zn(II) or Cd(II) centers, which effectively enhances the rigidity of the ligands and reduces the loss of energy via radiationless pathways [23].

4.3. *Magnetic properties of 3*

The magnetic susceptibility (χ) of **3** was measured on a powder sample under 1 kOe from 2–300 K (figure S3). The data above 25 K follow the Curie–Weiss law with $C = 3.28\ cm^3 K\ mol^{-1}$ and $\theta = -36.14$ K. The $\chi_M T$ value per Co(II) at 300 K is 3.04 emu K mol^{-1}, which is much larger than the spin-only value 1.88 emu K mol^{-1} for a magnetically active Co(II) ion ($S = 3/2$, $g = 2.0$), as expected for Co(II) systems with a significant contribution from the effects of spin-orbital coupling. As the temperature is lowered, the value of $\chi_M T$ decreases smoothly until 6 K. This may be attributed to the single-ion behavior of the Co(II). With a continued decrease in T to 2 K, the value of $\chi_M T$ increases smoothly. This effect is due to the presence of intramolecular weak ferromagnetism caused by small uncompensated AF spin-canting.

4.4. *Thermal stability of 1–3*

Thermal properties of **1–3** were investigated by TG experiments (figure S4). Compound **1** has no coordinated or interstitial solvent molecules, and hence, no mass loss was observed between 77–331 °C. The residual framework started to decompose at 331 °C in a series of complicated weight losses, and weight loss had not stopped when heating ended at 1000 °C. The TG curve of **2** suggests that the first weight loss of 4.01% between 77 and 183 °C corresponds to the release of the coordinated water molecules (calculated, 4.09%). The residual framework decomposed beyond 313 °C in a series of complicated weight losses and was still continuing when heating ended at 1000 °C. The TG curve of **3** suggests that the first weight loss of 3.30% between 77 and 180 °C corresponds to the release of the lattice water molecule (calculated 3.48%). The second weight loss of 13.87% between 250 and 280 °C likely involves the coordinated water molecule and an undeterminable fragment of one of the ligands. The residual framework decomposed beyond 350 °C in a series of complicated weight losses up to 800 °C.

5. Conclusion

In this study, we have presented the synthesis and crystal structure of three 2-D coordination polymers using carboxylate H_2L and three positionally isomeric dipyridyl bridging ligands (4,4′-bpt, 3,4′-bpt, and 3,3′-bpt) in combination with Zn(II), Cd(II) and Co(II) salts. Similar to reported benzenedicarboxylate complexes [1e,13,16,17,22], the aromatic dicarboxylate linker L adopted various coordination modes. Solid-state fluorescence spectra of **1** and **2** were recorded at room temperature. The maximum emission bands are at 414 nm (λ_{ex} = 358 nm) and 392 nm (λ_{ex} = 314 nm), respectively, which should arise from intraligand $\pi \rightarrow \pi^*$ transitions. For **3**, a weak ferromagnetic interaction was observed between the Co(II)

atoms bridged through the *syn-anti* carboxylate bridges. These results demonstrate that the bpt isomers can serve as bridging ligands to construct novel supermolecular architectures and illustrate the isomeric effect of bpt ligands in molecular tectonics of coordination polymers.

Supplementary data

Figures of experimental and simulated PXRD patterns and TG curves for **1–3**, solid state excited and emission spectra for **1** and **2**, and magnetic susceptibility data for **3**. CCDC 873592–873594 contains the supplementary crystallographic data for this article. These data can be obtained free of charge via http://www.ccdc.cam.ac.uk/data_ request/cif.

Acknowledgements

We gratefully acknowledge the National Nature Science Foundation of China (Nos. 21061002, 21101035), Guangxi Natural Science Foundation of China (2010GXNSF F013001, 2012GXNSFAA053035, 2012GXNSFBA053017) and the Nature Science Foundation of Guangxi Normal University.

References

[1] (a) P. Chaudhuri, V. Kataev, B. Büchner, H.H. Klauss, B. Kersting, F. Meyere. *Coord. Chem. Rev.*, **253**, 2261 (2009). (b) E. Coronado, P. Day. *Chem. Rev.*, **104**, 5419 (2004). (c) M.C. Dul, E. Pardo, R. Lescouëzec, Y. Journaux, J.F. Soria, R.R. García, J. Cano, M. Julve, F. Lloret, D. Cangussu, C.L.M. Pereira, H.O. Stumpf, J. Pasán, C. Pérez. *Coord. Chem. Rev.*, **254**, 2281 (2010). (d) G. Margraf, T. Kretz, F.F. Biani, F. Lashi, S. Losi, P. Zanello, J.W. Bats, B. Wolf, K.R. Langer, M. Lang, A. Prokofiev, W. Assmus, H.W. Lerner, M. Wagner. *Inorg. Chem.*, **45**, 1277 (2006). (e) K. Akhbari, A. Morsali. *J. Coord. Chem.*, **64**, 3521 (2011).

[2] (a) B. Cage, F.A. Cotton, N.S. Dalal, E.A. Hillard, B. Rakvin, C.M. Ramsey. *J. Am. Chem. Soc.*, **125**, 5270 (2003). (b) I.A. Koval, H. Akhideno, S. Tanase, C. Belle, C. Duboc, E.S. Aman, P. Gamez, D.M. Tooke, A.L. Spek, J.L. Pierre, J. Reedijk. *New J. Chem.*, **31**, 512 (2007). (c) H.A. Brison, T.P. Pollagi, T.C. Stoner, S.J. Geib, M.D. Hopkins. *Chem. Commun.*, 1263 (1997). (d) G.-Q. Zhang, G.-Q. Yang, J.-S. Ma. *Cryst. Growth Des.*, **6**, 375 (2006).

[3] (a) Y.-L. Wang, D.-Q. Yuan, W.-H. Bi, X. Li, X.-J. Li, F. Li, R. Cao. *Cryst. Growth Des.*, **5**, 1849 (2005). (b) Y.-B. Lu, M.-S. Wang, W.-W. Zhou, G. Xu, G.-C. Guo, J.-S. Huang. *Inorg. Chem.*, **47**, 8935 (2008). (c) O. Fabelo, J. Pasan, F. Lloret, M. Julve, C.R. Perez. *Inorg. Chem.*, **47**, 3568 (2008).

[4] (a) W.-G. Lu, L. Jiang, X.-L. Feng, T.-B. Lu. *Cryst. Growth Des.*, **8**, 986 (2008). (b) A.-X. Tian, J. Ying, J. Peng, J.-Q. Sha, H.-J. Pang, P.-P. Zhang, Y. Chen, M. Zhu, Z.-M. Su. *Inorg. Chem.*, **48**, 100 (2009).

[5] (a) Y. Wang, X.-Q. Zhao, W. Shi, P. Cheng, D.-Z. Liao, S.-P. Yan. *Cryst. Growth Des.*, **9**, 2137 (2009). (b) J. Park, S. Hong, D. Moon, M. Park, K. Lee, S. Kang, Y. Zou, R.P. John, G.H. Kim, M.S. Lah. *Inorg. Chem.*, **46**, 10208 (2007). (c) C.-H. Li, K.-L. Huang, Y.-N. Chi, X. Liu, Z.-G. Han, L. Shen, C.-W. Hu. *Inorg. Chem.*, **48**, 2010 (2009).

[6] (a) Y. Tao, J.-R. Li, Q. Yu, W.-C. Song, X.-L. Tong, X.-H. Bu. *CrystEngComm.*, **10**, 699 (2008). (b) B. Zheng, H. Dong, J. Bai, Y. Li, S. Li, M. Scheer. *J. Am. Chem. Soc.*, **130**, 7778 (2008).

[7] F.-P. Huang, J.-L. Tian, W. Gu, X. Liu, S.-P. Yan, D.-Z. Liao, P. Cheng. *Cryst. Growth Des.*, **10**, 1145 (2010).

[8] Y.-Q. Lan, S.-L. Li, J.-S. Qin, D.-Y. Du, X.-L. Wang, Z.-M. Su, Q. Fu. *Inorg. Chem.*, **47**, 10600 (2008).

[9] F.-P. Huang, J.-L. Tian, G.-J. Chen, D.-D. Li, W. Gu, X. Liu, S.-P. Yan, D.-Z. Liao, P. Cheng. *CrystEngComm.*, **12**, 1269 (2010).

[10] F. Bentiss, M. Lagrenee, M. Traisnel, B. Mernari, H. Elattari. *J. Heterocycl. Chem.*, **36**, 149 (1999).

[11] G.M. Sheldrick. *SHELXL97, Program for X-ray Crystal Structure Solution*, University of Göttingen, Göttingen (1997).

[12] J.E.V. Babb, A.D. Burrow, R.W. Harrington, M.F. Mahon. *Polyhedron*, **22**, 673 (2003).

[13] (a) W.-L. Zhang, Y.-Y. Liu, J.-F. Ma, H. Jiang, J. Yang. *Polyhedron*, **27**, 3351 (2008). (b) P. Zhang, D.-S. Li, J. Zhao, Y.-P. Wu, C. Li, K. Zou, J.Y. Lu. *J. Coord. Chem.*, **64**, 2329 (2011). (c) L.-N. Yang, Y.-X. Zhi, J.-H. Hei, J. Li, F.-X. Zhang, S.-Y. Gao. *J. Coord. Chem.*, **64**, 2912 (2011). (d) L. Tian, L. Yan, S.-Y. Liu. *J. Coord. Chem.*, **64**, 2945 (2011).
[14] X.-F. Xie, S.-P. Chen, Z.-Q. Xia, S.-L. Gao. *Polyhedron*, **28**, 679 (2009).
[15] (a) Z.-X. Li, Y.-F. Zeng, H. Ma, X.-H. Bu. *Chem. Commun*., **46**, 8540 (2010). (b) X.-F. Wang, Y.-B. Zhang, W. Xue, X.-L. Qi, X.-M. *Chen. Cryst. Eng. Comm.*, **12**, 3834 (2010).
[16] D. Zhao, Y. Xiu, X.-L. Zhou, X.-R. Meng. *J. Coord. Chem.*, **65**, 112 (2012).
[17] H.Y. Lin, B. Mu, X.L. Wang. *J. Coord. Chem.*, **64**, 3465 (2011).
[18] (a) F.-P. Huang, J.-L. Tian, W. Gu, S.-P. Yan. *Inorg. Chem. Commun.*, **13**, 90 (2010). (b) F.-P. Huang, J.-L Tian, D.-D. Li, G.-J. Chen, W. Gu, S.-P. Yan, X. Liu, D.-Z. Liao, P. Cheng. *Inorg. Chem.*, **49**, 2525 (2010). (c) F.-P. Huang, J.-L. Tian, D.-D. Li, G.-J. Chen, W. Gu, S.-P. Yan, X. Liu, D.-Z. Liao, P. Cheng. *Cryst. Eng. Comm*., **12**, 395 (2010). (d) F.-P. Huang, J.-B. Lei, Q. Yu, H.-D. Bian, S.-Pi. Yan. *Polyhedron*, **34**, 129 (2012). (e) Q. Zhang, F.-P. Huang, H.-D. Bian, Q. Yu. *J. Coord. Chem.*, **64**, 2110 (2011). (f) F.-P. Huang, H.-Y. Li, Q. Yu, H.-D. Bian, J.-L. Tian, S.-P. Yan, D.-Z. Liao, P. Cheng. *Cryst. Eng. Comm.*, **14**, 4756 (2012). (g) F.-P. Huang, Q. Zhang, Q. Yu, H.-D. Bian, H. Liang, S.-P. Yan, D.-Z. Liao, P. Cheng. *Cryst. Growth Des.*, **12**, 1890 (2012).
[19] (a) Z.-X. Li, Y.-F. Zeng, H. Ma, X.-H. Bu. *Chem. Commun.*, **46**, 8540 (2010). (b) X.-H. Bu, M.-L. Tong, J.-R. Li, H.-C. Chang, L.-J. Li, S. Kitagawa. *Cryst. Eng. Comm*., **7**, 411 (2005).
[20] (a) Q. Wu, M. Esteghamatian, N.-X. Hu, G. Enright, Y. Tao, M. Díorio, S. Wang. *Chem. Mater.*, **12**, 79 (2000). (b) J.E. McGarrah, Y.J. Kim, M. Hissler, R. Eisenberg. *Inorg. Chem.*, **40**, 4510 (2001). (c) G.D. Santis, L. Fabbrizzi, M. Licchelli, A. Poggi, A. Taglietti. *Angew. Chem. Int. Ed. Engl.*, **35**, 202 (1996). (d) C. Seward, W.L. Jia, R.Y. Wang, G.D. Enright, S. Wang. *Angew. Chem. Int. Ed.*, **43**, 2933 (2004). (e)
S.-L. Zheng, J.-H. Yang, X.-L. Yu, X.-M. Chen, W.-T. Wong. *Inorg. Chem.*, **43**, 830 (2004). (f) R.-H. Wang, L. Han, F.-L. Jiang, Y.-F. Zhou, D.-Q. Yuan, M.-C. Hong. *Cryst. Growth Des.*, **5**, 129 (2005).
[21] S.-M. Fang, Q. Zhang, M. Hu, X.-G. Yang, L.-M. Zhou, M. Du, C.-S. Liu. *Cryst. Growth Des.*, **10**, 4773 (2010).
[22] (a) M. Du, X-J. Jiang, X.-J. Zhao. *Inorg. Chem.*, **45**, 3998 (2006). (b) L.-J. Li, G. Yuan, L. Chen, D.-Y. Du, X.-L. Wang, G.-J. Xu, H.-N. Wang, K.-Z. Shao, Z.-M. Su. *J. Coord. Chem.*, **64**, 1578 (2011).
[23] (a) J.-J. Wang, C.-S. Liu, T.-L. Hu, Z. Chang, C.-Y. Li, L.-F. Yan, P.-Q. Chen, X.-H. Bu, Q. Wu, L.-J. Zhao, Z. Wang, X.-Z. Zhang. Cryst. Eng. Comm., **10**, 681 (2008). (b) B. Valeur, *Molecular Fluorescence: Principles and Applications*, Wiley-VCH (2002).